

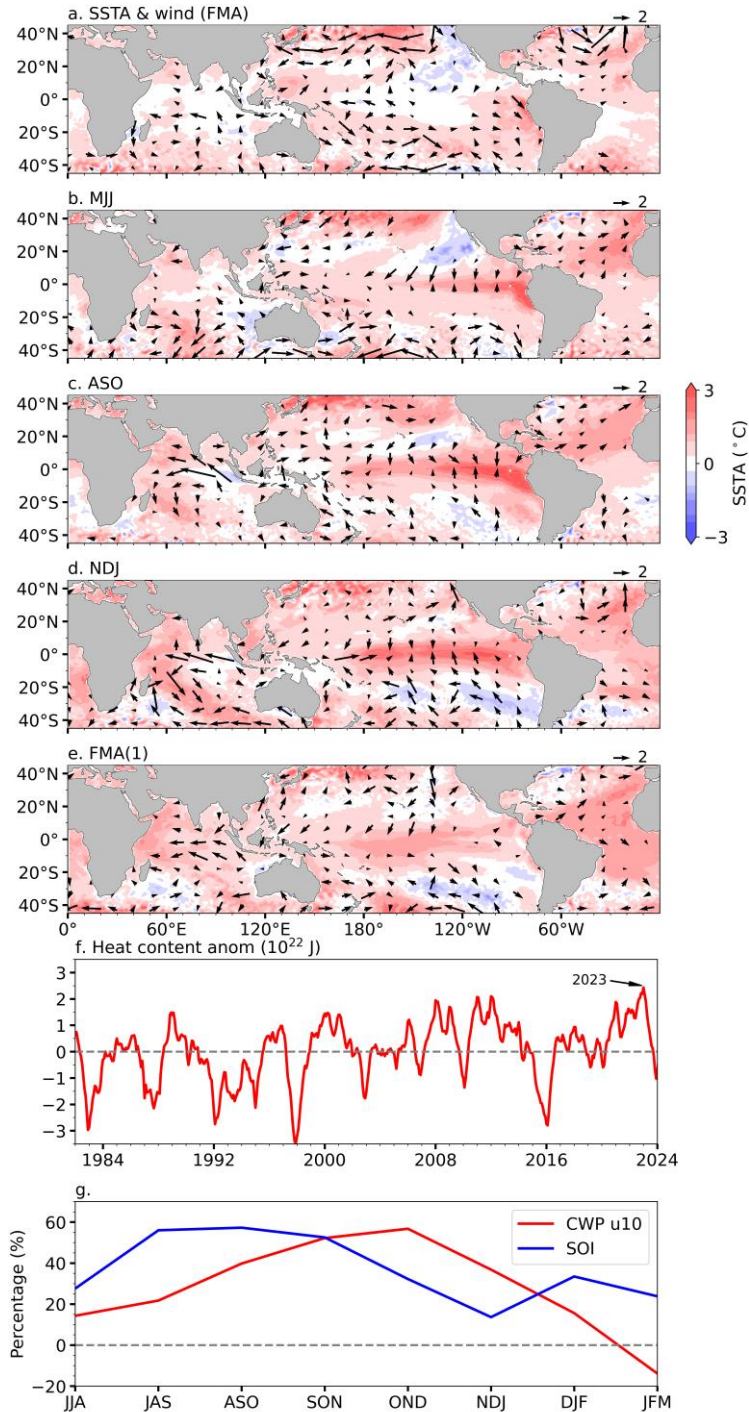
1

Extended Data Table 1 | Description of the AGCM experiments

Experiments	Forcings	Description
aCTRL	Climatological SST+2023 SSTA	All 2023 SSTA included
aPac	Climatological SST+2023 Pacific detrended SSTA	Impacts of 2023 Pacific detrended SSTA
aIndAtl	Climatological SST+2023 Indian-Atlantic detrended SSTA	Impacts of Indian-Atlantic detrended SSTA
aTrend	Climatological SST+ Global SST trend	Impacts of global SST trend
aPac_RSST	Climatological SST+2023 Pacific relative SSTA	Impacts of 2023 Pacific relative SSTA

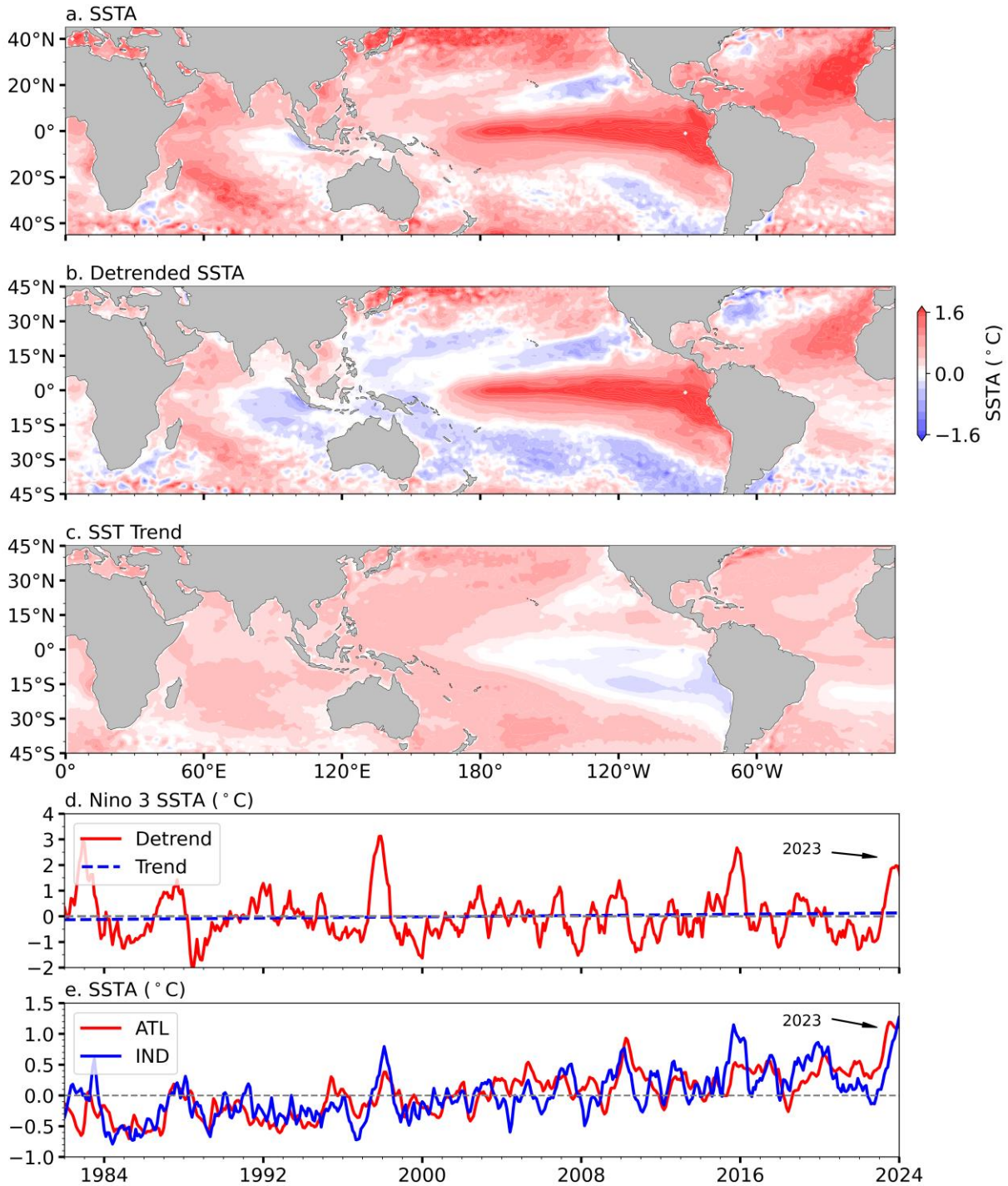
2

Experiments	Wind stress	Description
CTRL	Daily ERA5 wind stress during 1941-2023.	All processes included
InitApr2023	Initialized on 1 April 2023. 31-day running-mean wind stress anomalies are removed after 1 April 2023. High-frequency wind stress anomalies within 31-day are retained.	Impacts of initial conditions on the 2023-24 El Niño
Wind2023	-	Derived as the difference, CTRL-InitApr2023 . The result indicates the impacts of wind stress anomalies in 2023
InitAprOther	Same as InitApr2023, but 31-day running-mean wind stress anomalies are removed after Apr 1 in other comparable El Niños of 1982/83, 1997/98, and 2015/16. High-frequency wind stress anomalies within 31-day are retained.	Impacts of initial conditions on the other comparable El Niño events
WindOther	-	Derived as the difference, CTRL-InitAprOther . The result indicates the impacts of wind stress anomalies in the other comparable El Niño events
InitApr2023_noHighfreq	Same as InitApr2023, but high-frequency wind stress anomalies within 31-day are removed.	Evaluate the effect of high-frequency wind stress within 31 days on the 2023-24 El Niño by comparing the results with those from InitApr2023
InitAprOther_noHighfreq	Same as InitAprOther, but high-frequency wind stress anomalies within 31-day are removed.	Assess the impacts of high-frequency wind stress within 31 days on the other comparable El Niño events by comparing the results with those from InitAprOther



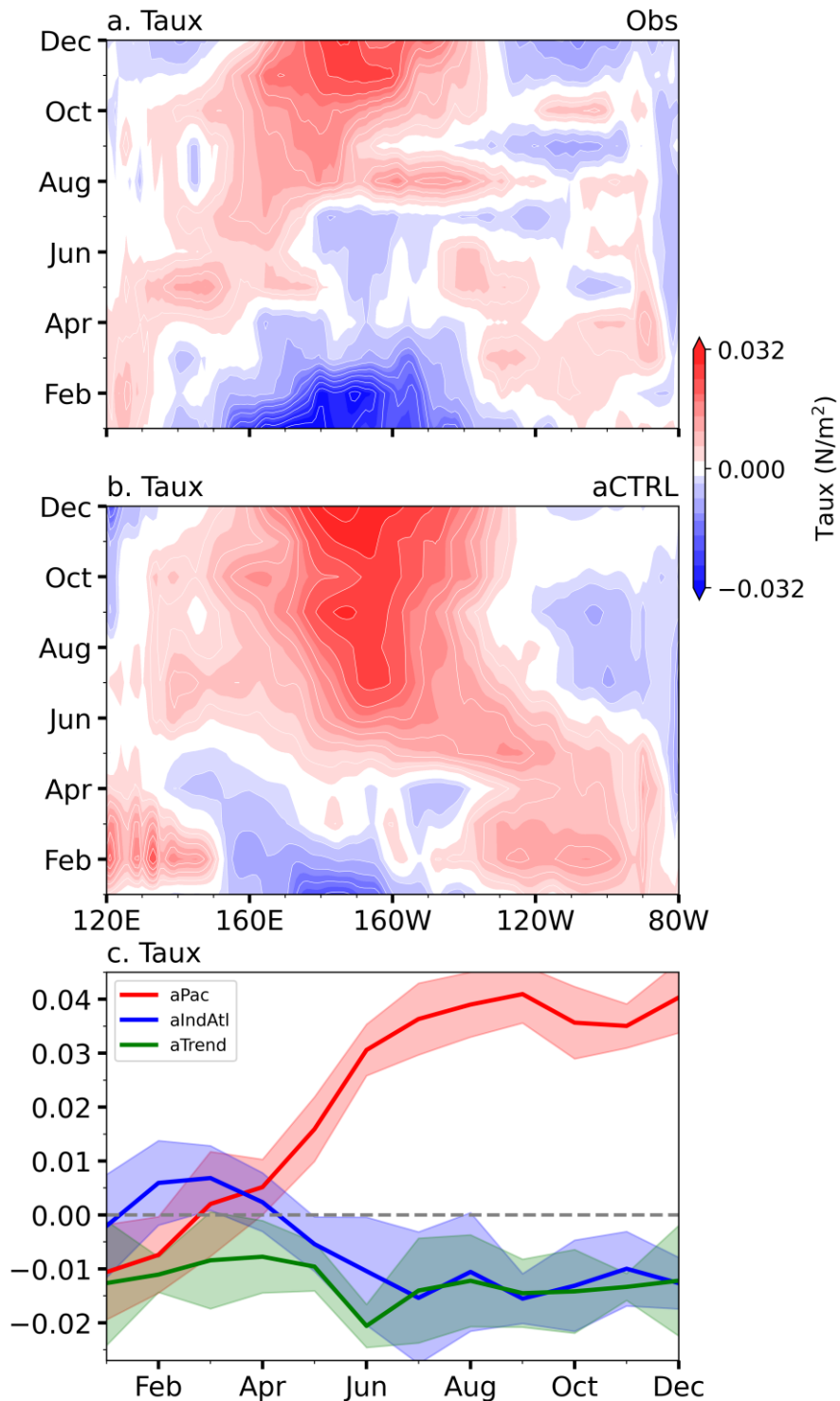
4

5 **Extended Data Fig. 1 | Evolution of SSTA and 10-m wind anomalies during 2023-24.**
 6 Observed SSTA (°C, color shading) and 10-m wind anomalies (m/s, vectors) averaged in (a)
 7 February-April (FMA), (b) May-July (MJJ), (c) August-October (ASO), (d) November-January
 8 (1) (NDJ), and (e) FMA 2024. Time series of (f) upper-300 m OHC anomalies (10^{22} J) in the
 9 western Pacific Ocean (WPAC, 130°E–180°, 10°S–10°N) and (g) percentage of 2023–24
 10 observed CWP u10 and SOI compared to their expected values derived from regression analysis.
 11 All anomalies are defined relative to the period 1982-2022.



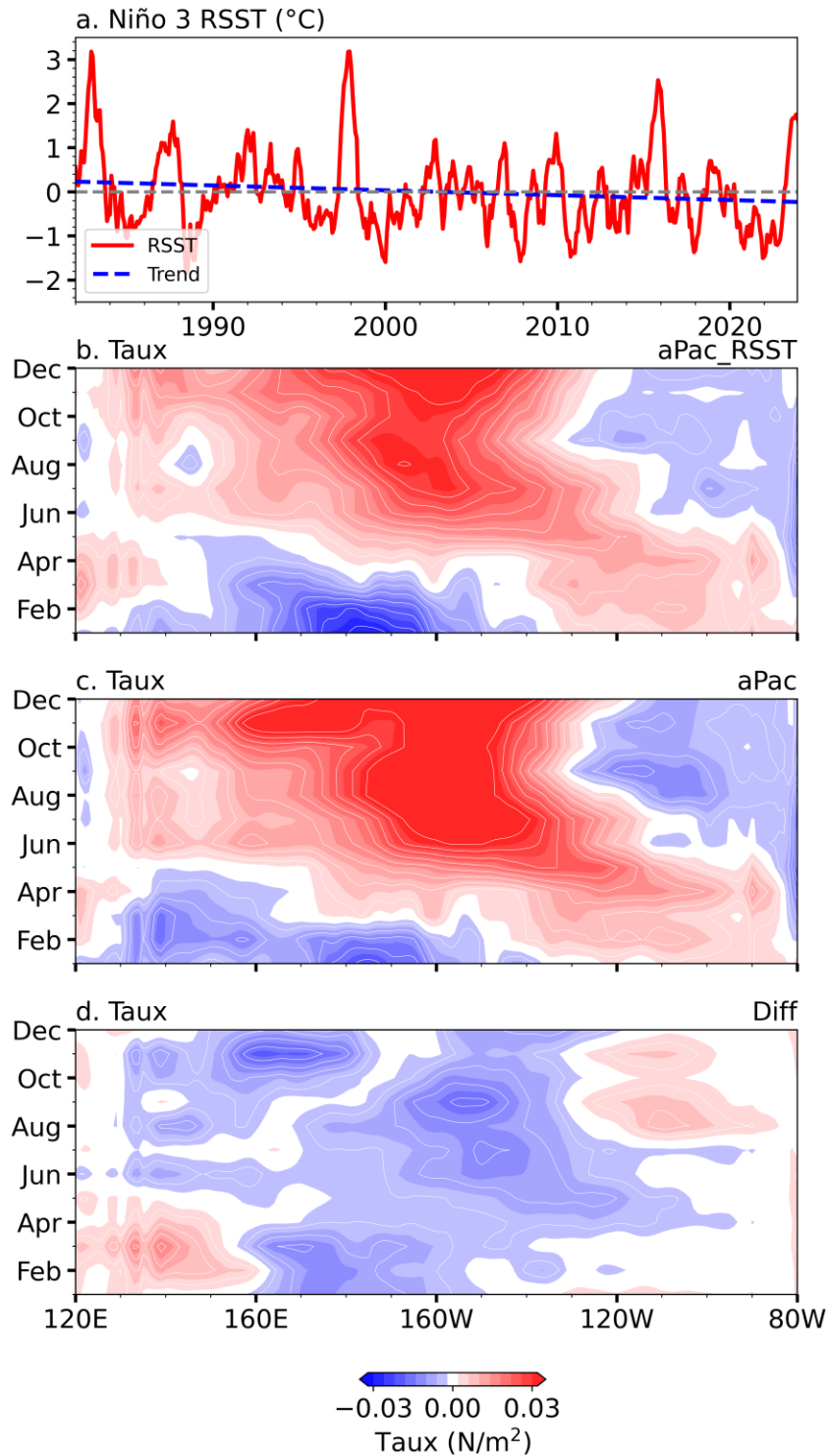
12

13 **Extended Data Fig. 2 | Decomposition of observed SSTA for the AGCM experiments.** The
 14 June-December 2023 averaged (a) SSTA (°C), (b) detrended SSTA component, and (c) the
 15 background SST trend component for the period 1982-2023, obtained by subtracting (b) from
 16 (a). All anomalies are calculated with reference to the 1982-2022 climatological values. Time
 17 series of (d) detrended and trended Niño3 index as well as (e) SSTAs averaged over the tropical
 18 North Atlantic (0-70°W, equator-30°N) and tropical western Indian Ocean (40°E-70°E, 10°S-
 19 10°N).



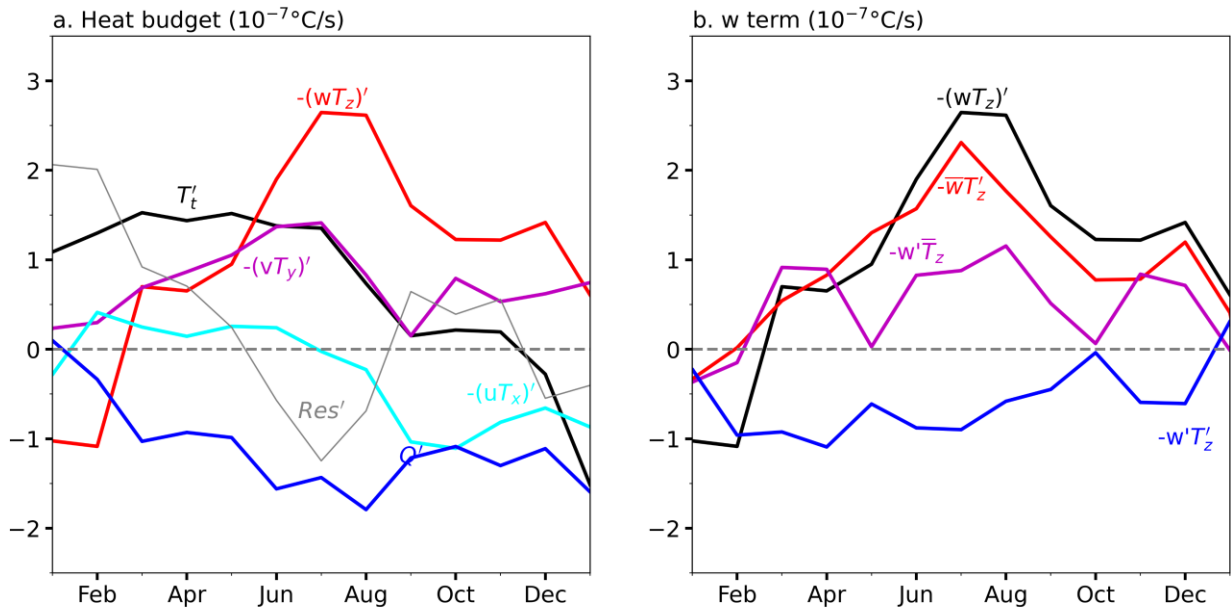
20

21 **Extended Data Fig. 3 | Observed and simulated surface wind stress changes.** Hovmöller
 22 diagram of equatorial zonal wind stress anomalies (color shading; N/m^2) from (a) observations
 23 and (b) aCTRL. (c) Time series of central Pacific ($170^\circ W$ - $150^\circ W$, $2^\circ S$ - $2^\circ N$) zonal wind stress
 24 responses from aPac, aIndAtl, and aTrend runs. The line represents the ensemble mean, and the
 25 shading indicates one inter-member s.d..



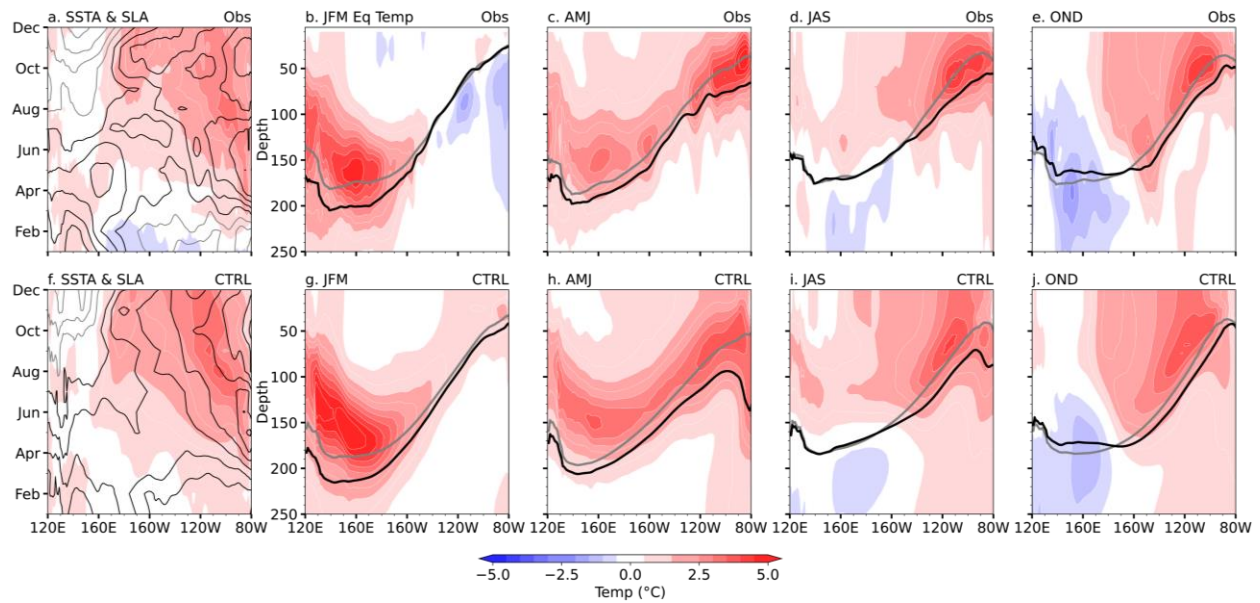
26

27 **Extended Data Fig. 4 | Impacts of Pacific relative SST.** (a) Time series of Niño3 relative SST,
 28 including the long-term trend shown in blue. Hovmöller diagram of equatorial zonal wind stress
 29 anomalies (color shading; N/m²) from (b) aPac_RSST, (c) aPac, and (d) their differences.

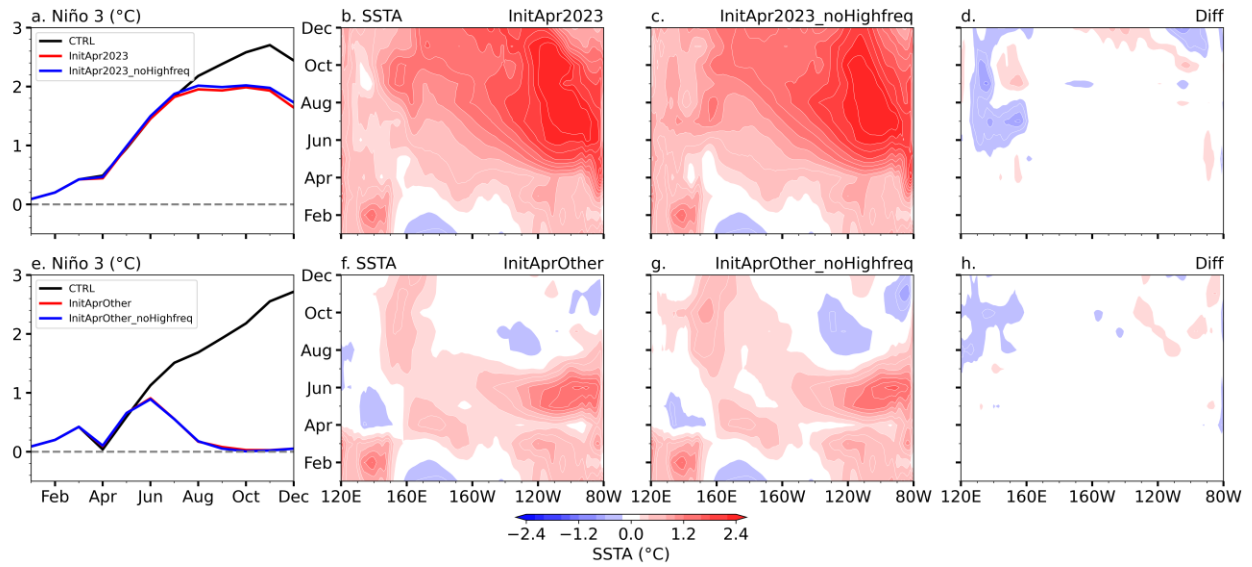


30

31 **Extended Data Fig. 5 | The mixed layer heat budget for the 2023-24 El Niño.** (a) Heat budget
 32 terms of the 2023-24 El Niño (10^{-7}C/s , averaged in Niño 3 region) (see Materials and Methods).
 33 (b) The relative importance of thermocline feedback (TH, red line), Ekman feedback (EK,
 34 magenta line), and the nonlinear term (blue line) in modulating the vertical advection term.
 35 These results are derived from reanalysis data.

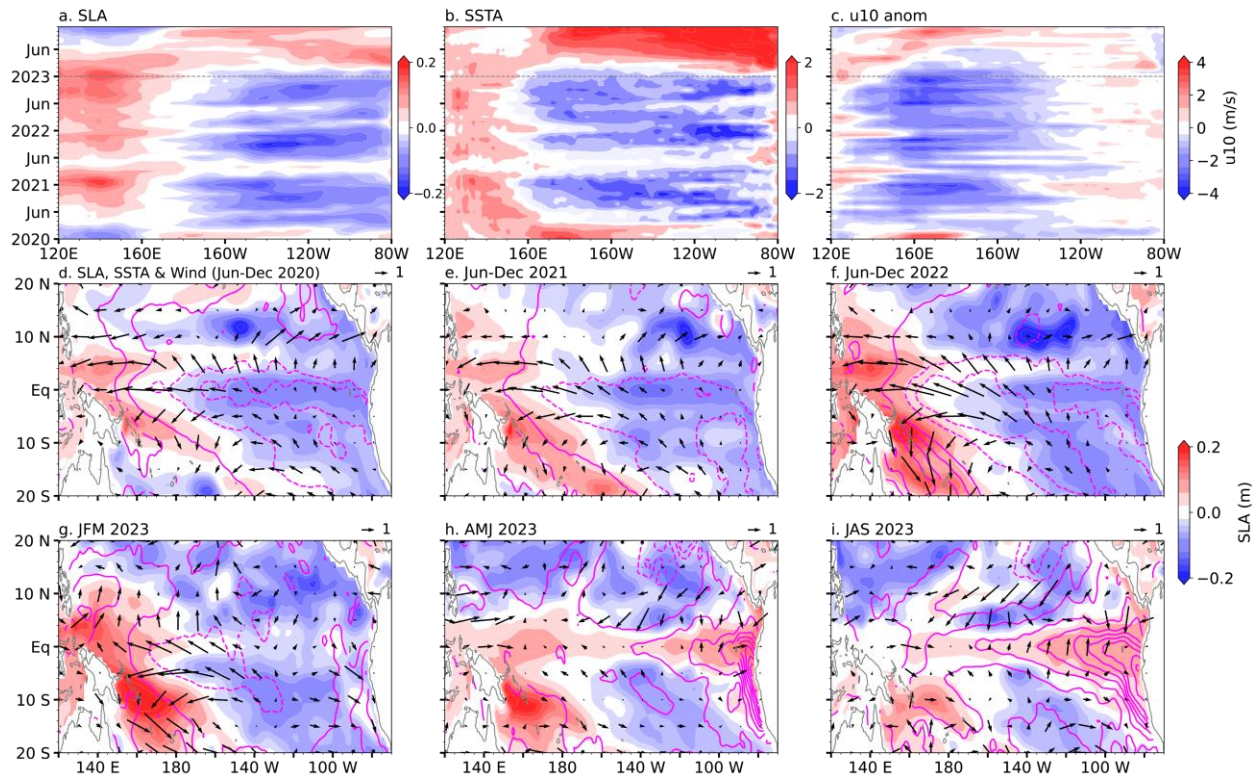


36
 37 **Extended Data Fig. 6 | Comparison of the observed and simulated subsurface ocean**
 38 **temperature anomalies for the 2023-24 event.** (a) Longitude-time diagram of observed
 39 equatorial SSTAs (color shading; °C) and SLAs (contours with an interval of 3 cm; positive
 40 black and negative gray). (b)-(e) shows the evolution of observed equatorial ocean temperature
 41 anomalies (°C, color shading) for the 2023-24 El Niño averaged over (a) January-March (JFM),
 42 (b) April-June (AMJ), (c) July-September (JAS), and (d) October-December (OND). The lower
 43 panels are similar to the upper panels but from the CTRL run. The black (grey) line represents
 44 the 2023 (climatological) 20 °C isotherm. All meridionally averaged over 2°S–2°N.



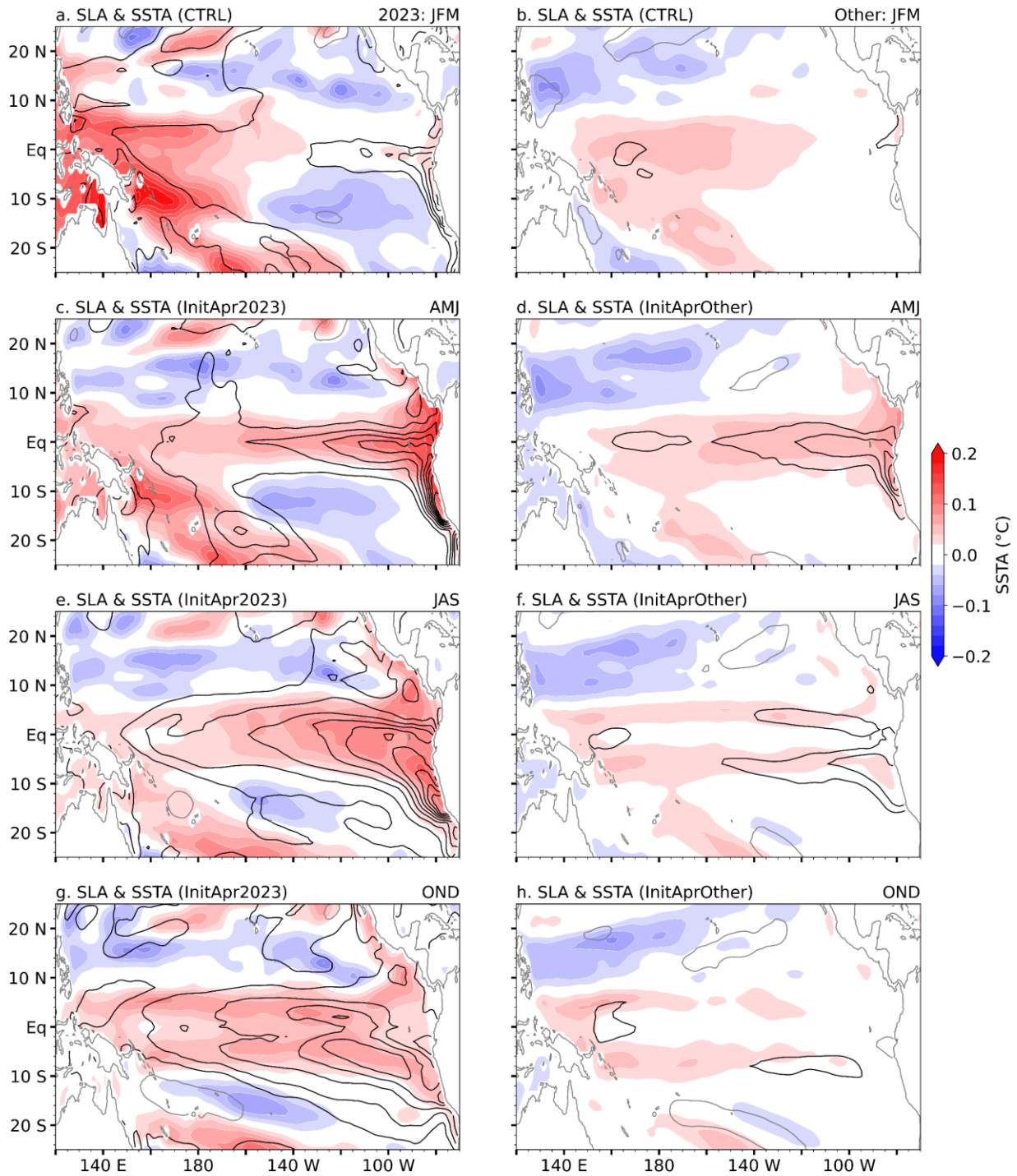
45

46 **Extended Data Fig. 7 | The impacts of high-frequency wind stress.** (a) Simulated Niño 3
 47 SSTAs from the CTRL, InitApr2023, and InitApr2023_noHighfreq experiment. Hovmöller
 48 diagram of equatorial SSTA (color shading) from the (b) InitApr2023, (c)
 49 InitApr2023_noHighfreq, and (d) their differences. (Lower panels) Same as (Upper panels) but
 50 for the composite results of the other comparable El Niños from CTRL, InitAprOther, and
 51 InitAprOther_noHighfreq. Note that only the first member of each experiment is shown here.



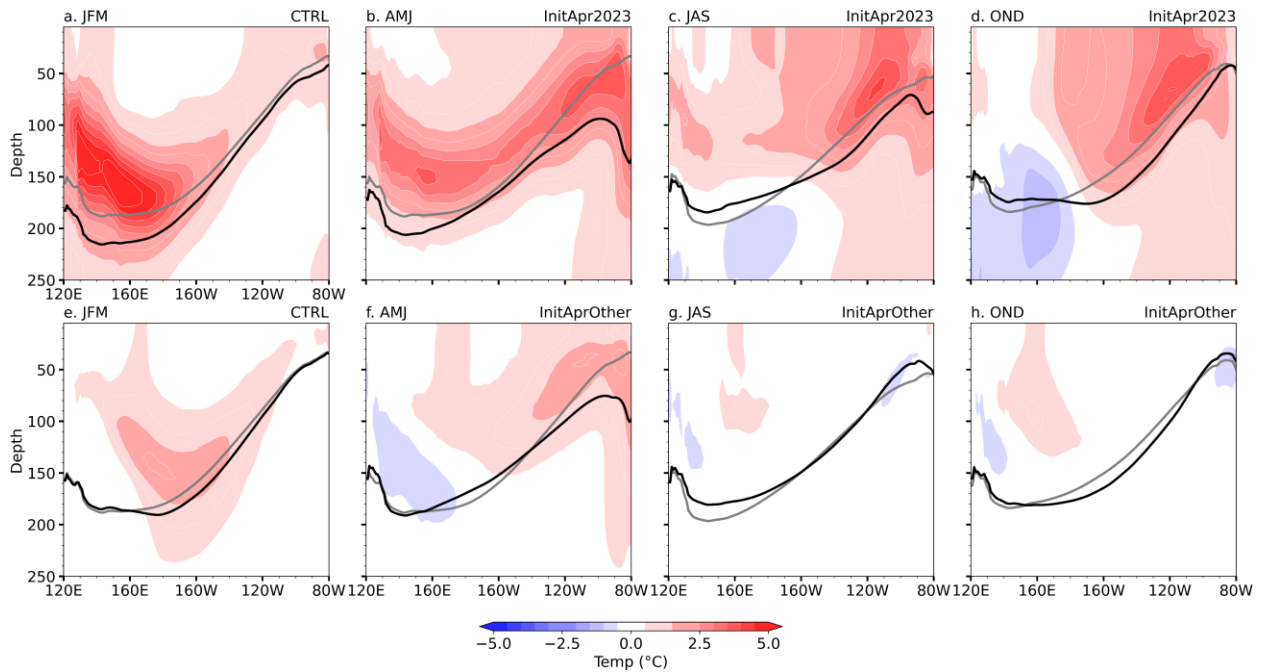
52

53 **Extended Data Fig. 8 | Observed climate state during 2020-2023.** Longitude-time evolution of
 54 the (a) equatorial SLA (m), (b) SSTA ($^{\circ}\text{C}$), and (c) 10-m zonal wind anomalies (m/s) during
 55 January 2020-December 2023. All meridionally averaged over 2°S – 2°N . (d)–(f) Observed SLA
 56 (m, color shading), SSTA (contours with a 0.2°C interval), and surface wind anomalies (m/s,
 57 vectors) averaged over June–December for the years 2020, 2021, and 2022, respectively. The
 58 lower panels are similar to the middle panels but averaged in (g) JFM, (h) AMJ, and (i) JAS
 59 2023, respectively.



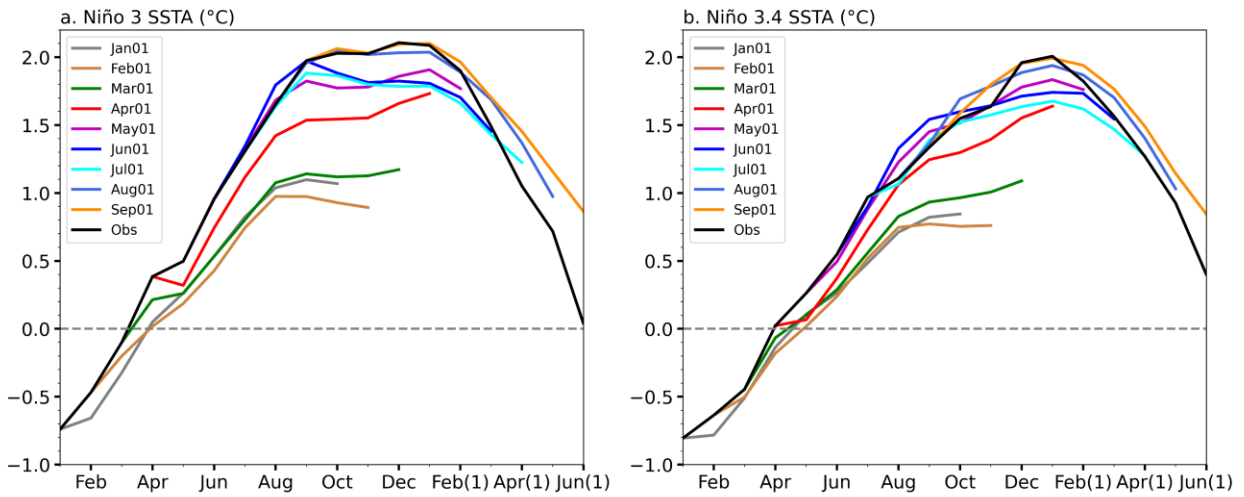
60

61 **Extended Data Fig. 9 | The impacts of initial condition on the 2023-24 and other**
 62 **comparable El Niños.** Simulated SLA (m, color shading) and SSTA (contours with an interval
 63 of 0.5 °C; positive black and negative gray) in (c) January-March (JFM) 2023 from the CTRL
 64 Run, which roughly describes the initial condition for the InitApr2023. (e), (g), and (i) same as
 65 (c) but averaged in (e) AMJ, (g) JAS, and (i) OND from the InitApr2023 experiment. The right
 66 panels are similar to the left panels but for other comparable El Niño composites from the
 67 InitAprOther run.



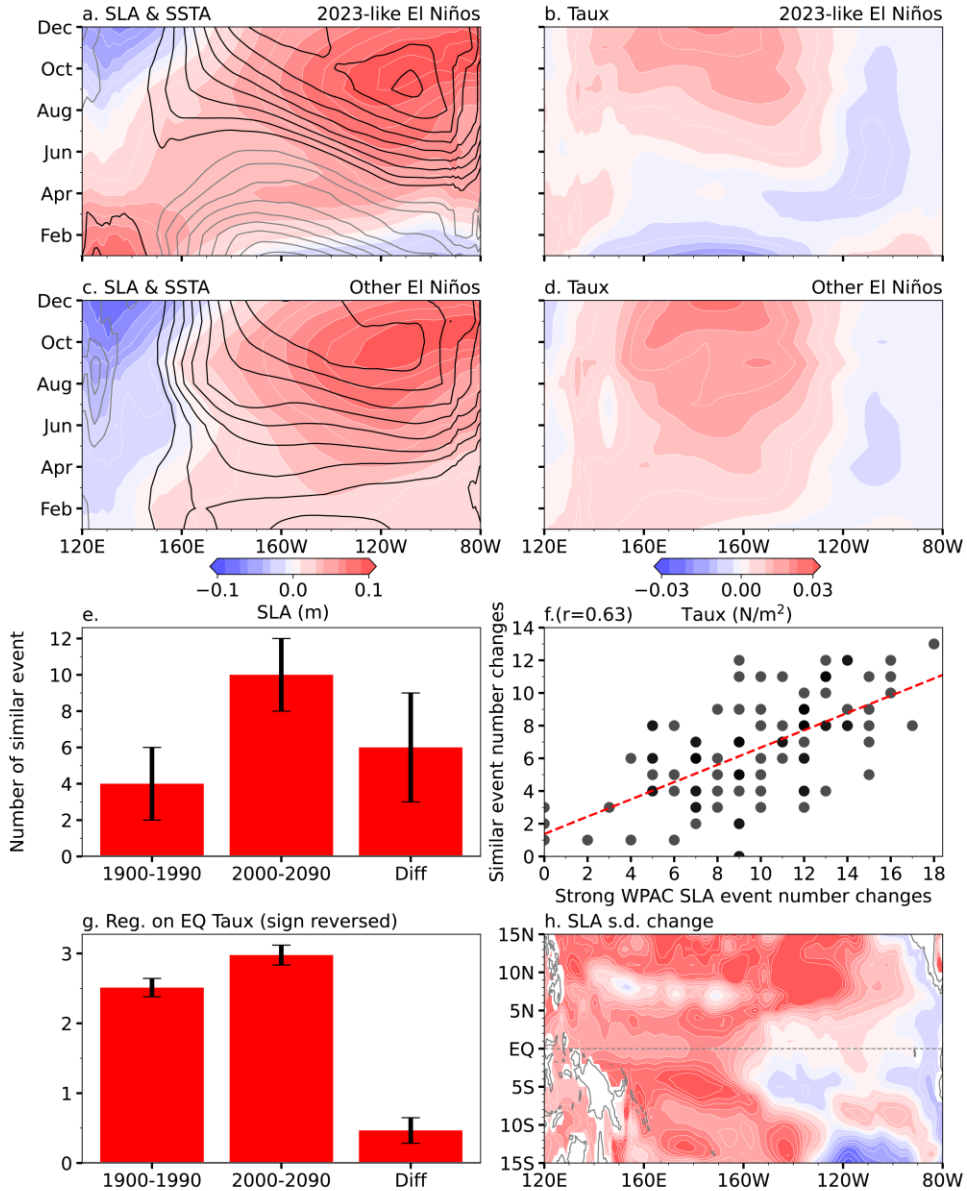
68

69 **Extended Data Fig. 10 | Equatorial temperature changes from the InitApr2023 and**
 70 **InitAprOther experiments.** (a) The JFM ocean temperature anomalies from the CTRL run,
 71 which generally describes the initial condition for the InitApr2023. (b)-(d) The evolutions of
 72 equatorial ocean temperature anomalies averaged over (a) JFM, (b) AMJ, (c) JAS, and (d) OND
 73 from InitApr2023. Lower panels are similar to upper panels but for the other comparable El Niño
 74 composite (InitAprOther). The black (grey) line represents the 2023 (climatological) 20 °C
 75 isotherm. All panels are meridionally averaged over 2°S–2°N.



76

77 **Extended Data Fig. 11 | NMME predictions for the 2023-24 El Niño.** Seasonal forecast for
 78 (a) Niño 3.4 and (b) Niño 3 SSTA (°C) from NMME. Each colored line denotes the multi-model
 79 ensemble averages of a specific forecast. The start of each curve indicates the month of the
 80 forecast's initialization. For example, the red line represents the forecast initialized on April 1,
 81 2023. Observations are plotted in black.



82

83 **Extended Data Fig. 12 | Future changes in 2023-like El Niños.** Hovmöller diagram of
 84 equatorial (a) SLA (m, color shading) and SSTA ($^{\circ}\text{C}$, contours with an interval of $0.2\text{ }^{\circ}\text{C}$; positive
 85 black and negative gray), and (b) zonal wind stress (color shading; N/m^2) for the 2023-like El
 86 Niño composites during 1900-1990. (c)-(d) Same as (a)-(b) but for other non-2023-like El Niños.
 87 (e) Comparison of the number of 2023-like El Niño (see Materials and Methods) during 1900-
 88 1990 and 2000-2090, along with their differences. (f) Scatter plot for changes in the number of
 89 strong positive SLA events in the WPAC region during JFM (SLA $> 4.5\text{ cm}$) and changes in the
 90 number of 2023-like El Niño events. (g) Regression (sign reversed) of WPAC JFM SLA (m)
 91 onto the preceding August (-1)-January equatorial (averaged over 130°E - 90°W and 2°S - 2°N)
 92 zonal wind stress anomalies (Taux) during 1900-1990 and 2000-2090, along with their
 93 differences. (a)-(g) are derived from the CESM-LENS2 simulations. (h) Simulated JFM
 94 interannual SLA s.d. percentage changes due to global warming, calculated as the difference
 95 between the Warming_{CESM} and CTRL_{CESM} experiments (see Methods).